Spangenberg, E., Seyberth, K., Heeschen, K., Priegnitz, M., Schicks, J. (2018): A Quick Look Method to Assess the Dependencies of Rock Physical Sediment Properties on the Saturation With Pore-Filling Hydrate. - *Journal of Geophysical Research*, *123*, 7, pp. 5588—5598.

DOI: http://doi.org/10.1029/2018JB015855

Journal of Geophysical Research: Solid Earth

RESEARCH ARTICLE
10.1029/2018JB015855

Special Section:
Gas Hydrate in Porous Media: Linking Laboratory and Field Scale Phenomena

A *Quick Look* Method to Assess the Dependencies of Rock Physical Sediment Properties on the Saturation With Pore-Filling Hydrate

Erik Spangenberg[1], Karl Seyberth[2], Katja U. Heeschen[1], Mike Priegnitz[3], and Judith M. Schicks[1]

[1]GFZ German Research Centre for Geosciences, Potsdam, Germany, [2]Karlsruhe Institute of Technology, Karlsruhe, Germany, [3]Texplor Exploration and Environmental Technology GmbH, Potsdam, Germany

Abstract Within the framework of the national German hydrate project Submarine Gas Hydrate Reservoirs (SUGAR) we promised to deliver dependencies of compressional-wave velocity and electrical resistivity on hydrate saturation within sand sediments of the paleo Danube channel-levee system in the Black Sea. These data supported starting models for joint inversion of seismic and electromagnetic geophysics data for that area. Because hydrate formation in sediment samples under laboratory conditions is a complex and particularly time-consuming procedure, we developed a *quick look* experimental methodology. We used ice as an analogue for methane hydrate to simplify the experimental procedure for laboratory studies. The difference from existing approaches is the way the ice and water saturation of the porous sediment is determined. To verify this approach, we compared the new data measured on ice-bearing sand with measurements on hydrate-bearing sediments, where methane hydrate was produced from methane dissolved in water. The main result from this study is that ice forming from a salt solution in the pore space of sand forms like methane hydrate as a noncementing solid pore fill. The method does not require a pore pressure system and produces a homogeneous ice distribution, as long as homogeneous temperature distribution throughout the sample can be guaranteed. For compressional-wave velocity measurements we demonstrate that ice can be used as an analogue for noncementing methane hydrate. Therefore, the complete dependence of velocity on ice saturation, depending on the saturation increment, can easily be measured in 1 to 2 weeks.

Key Points:
- Ice is used as replacement for methane hydrate in lab experiments measuring compressional-wave velocities
- Density and electrical resistivity of KCl solutions at freezing point have been measured as prerequisite for interpretation
- The dependencies of velocity on hydrate saturation and on ice saturation are in good agreement

Correspondence to:
E. Spangenberg,
erik@gfz-potsdam.de

Citation:
Spangenberg, E., Seyberth, K., Heeschen, K. U., Priegnitz, M., & Schicks, J. M. (2018). A *quick look* method to assess the dependencies of rock physical sediment properties on the saturation with pore-filling hydrate. *Journal of Geophysical Research: Solid Earth*, *123*, 5588–5598. https://doi.org/10.1029/2018JB015855

Received 29 MAR 2018
Accepted 21 JUN 2018
Accepted article online 28 JUN 2018
Published online 21 JUL 2018

1. Introduction

Gas hydrates are considered the largest resource for fossil fuel despite the estimates varying by several orders of magnitude (Boswell, 2009; Boswell et al., 2014). They occur in sediments along continental slopes and in permafrost regions where temperature, pressure, and a sufficient supply of methane gas allow for their formation (Kvenvolden, 1988). The ice-like water structures of gas hydrates encage large amounts of guest molecules; in nature this is mostly methane. Hydrates often form layers or nodules in fine sediments and occur disseminated in the pores of coarser sediments (Waite et al., 2009). Due to the higher permeabilities and higher gas hydrate saturations, coarser sediment layers are the target lithology for gas production from gas hydrates (Boswell et al., 2012, and references therein).

To investigate physical changes of gas hydrate-bearing sediments during gas production in the laboratory requires (a) pristine natural sediment samples from pressure coring or (b) artificial samples that mimic natural conditions. Studies on natural gas hydrate-bearing samples require the preservation of in situ conditions during core recovery, sample transformation, and measurements (Inada & Yamamoto, 2015; Schultheiss et al., 2009, 2011). Once pressure or temperature had been shifted outside the stability field even for a short time, an investigation of mechanical and physical properties will not provide the undisturbed information about the reservoir properties. Furthermore, natural samples only allow for single measurements at one hydrate saturation instead of a broad range of hydrate saturations, which is needed to derive the saturation dependence for a certain rock physical property. Therefore, many laboratory studies use artificial samples of sand and methane hydrate (see Waite et al., 2009, and references therein) or even tetrahydrofuran hydrates, which can be produced at standard pressure conditions (e.g., Cortes et al., 2009; Handa et al., 1984; Lee et al., 2007; Santamarina & Ruppel, 2010; Strauch et al., 2018; Yun et al., 2005).

Often the morphology of these hydrates used in laboratory studies is of a cementing nature caused by the formation of methane hydrates using the excess gas method with gas being introduced into a partially saturated or moist sediment (e.g., Hyodo et al., 2013; Priest et al., 2009; Waite et al., 2004). Natural samples,

however, are thought to mainly contain pore-filling hydrate or at high concentrations pore-filling and load-bearing gas hydrates. In the laboratory, these morphologies are commonly produced from methane-saturated solutions cycling through a sediment sample for a long period of time (Spangenberg et al., 2005; Waite & Spangenberg, 2013). This dissolution controlled method has earlier been described as a time-consuming process (Choi et al., 2014). Nevertheless, it is the pore-filling morphology and a homogeneous distribution throughout the sample that are needed to mimic natural conditions and gain useful information about the physical properties and mechanical behavior of the gas hydrate reservoirs (Priest et al., 2009; Spangenberg et al., 2014; Spangenberg & Kulenkampff, 2006). An overview of the different methods and their pros and cons is given by Waite et al. (2009).

Recently, Choi et al. (2014) suggested a method that allows the formation of the desired homogeneous pore-filling gas hydrates in just over a week. The authors used the *excess gas* method to form cementing hydrate followed by a water injection and a recrystallization process, redistributing the cementing hydrate into a pore-filing morphology. This method saves some time in attaining the target hydrate saturation but does only allow for measurements at that target hydrate content instead of providing the parameter's complete saturation dependency in a single test. In addition, high saturations are difficult to produce with both the *excess water* method and the excess gas method. Priest et al. (2009) realized a maximum saturation of about 40% using the excess water method, where Waite et al. (2004) produced a maximum hydrate saturation of 70% in about 58 days (1,400 hr) using the excess gas method.

Pearson et al. (1983) proposed an empirical relationship between the water saturation and the electric resistivity of gas hydrate-bearing sandy sediment. Based on the strong similarities between the physical properties of ice and gas hydrates, they used a test series of resistivity measurements of partially frozen sediments to evaluate the relevance and empirical constants of Archie's equation for partly *gas hydrate*-saturated samples (Archie, 1942). To produce the test series on sandstones, limestones, sands, and silts, the temperature of the initially brine-saturated samples was incrementally decreased (Pearson et al., 1983, and references therein). As a result ice—as a proxy for gas hydrate—and an increasingly saltier solution formed while simultaneously the freezing point depression of the residual solution increased. In the method presented here, we also used the Pearson et al. (1983) partial freezing approach, but the estimation of the ice content is different. In our method (1) we used the approach of Hall et al. (1988) to calculate the salinity of the used KCl solution at temperatures below freezing, (2) we incorporated the influence of volume expansion during ice formation into the saturation estimation, and (3) we determined the electrical fluid conductivity and the density of the KCl solution as a function of freezing point depression as a prerequisite for proper interpretation. Further, we applied a controlled confining pressure to avoid any pore volume increase due to the volume expansion during ice formation. To verify the method, we compared measurements of compressional-wave velocity and electrical resistivity using both ice and hydrate.

The motivation for the development of the *quick look* experiment methodology was provided by the German national hydrate project SUGAR. Within the framework of the SUGAR project we promised to deliver dependencies of compressional-wave velocity and electrical resistivity on hydrate saturation for different reservoir sands in different depths below sea floor to generate starting models for joint inversion of seismic and electromagnetic geophysics data for sediments of the Paleo Danube Delta. The main result from this study is that ice, forming from a salt solution in the pore space of sediments, forms like methane hydrate as a noncementing solid pore fill. For the compressional-wave velocities we could demonstrate that ice can be used as a hydrate analogue. For the dependencies of electrical resistivity on ice saturation we have no proof yet that ice will produce the same dependency as hydrate formed from dissolved phase methane and can be used as an analogue.

2. Theory

The method of partial ice freezing in a porous system is based on the freezing point depression of NaCl-KCl-H_2O solutions and uses the equations proposed by Hall et al. (1988). We use the notation of Hall et al. (1988). The salinity S in wt-% of a solution is given as a function of freezing point depression θ in °C:

$$S = \left\{ \frac{\theta}{2e} + \left[\left(\frac{\theta}{2e} \right)^2 + \left(\frac{C}{3e} \right)^3 \right]^{1/2} \right\}^{1/3} + \left\{ \frac{\theta}{2e} - \left[\left(\frac{\theta}{2e} \right)^2 + \left(\frac{C}{3e} \right)^3 \right]^{1/2} \right\}^{1/3}, \quad (1)$$

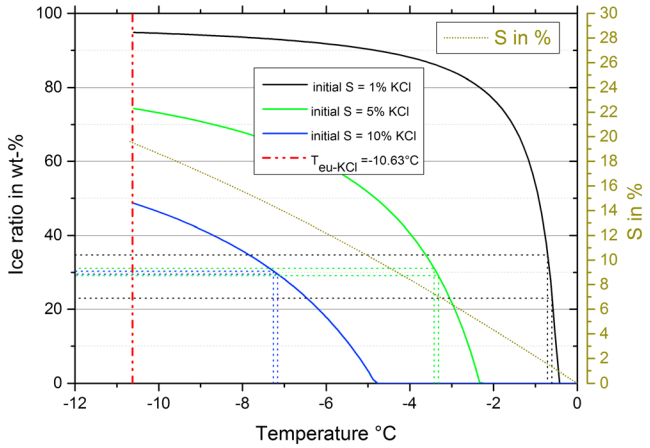

Figure 1. Increase of ice content with decreasing temperature for different initial salinities calculated using equations (1)–(4). The dashed lines show the influence of a temperature variation of 0.1 °C on the ice content (see text for explanation). The dotted line with an almost linear trend refers to the right axis and relates the salinity to the freezing point (after Hall et al., 1988).

C depends on the salt composition X in the form $C = 0.4597 + 0.1440\ X$, where X is the NaCl/(NaCl+KCl) ratio and the variable e follows from

$$e = 2.227\ 10^{-4} + 1.999\ 10^{-4}X + 4.633\ X^2 + 1.123\ 10^{-4}X^3.$$

In our experiments we used pure KCl ($X = 0$) solutions so that $C = 0.4597$ and $e = 2.227 \cdot 10^{-4}$. The basic idea is the use of equation (1) to relate a certain temperature below freezing to a certain salinity of the KCl solution. If this salinity is higher than that of the original solution, the salinity increase can be used to calculate the amount of ice that must have formed to account for that increase. We used pure KCl solution because the eutectic point (−10.69 °C) is higher than that of NaCl (−21.21 °C) (Hall et al., 1988). We start with an initial salinity S_0 of our KCl solution.

$$S_0 = \frac{m_{\mathrm{KCl}}}{m_{\mathrm{KCl}} + m_{\mathrm{H_2O}}} 100\%, \tag{2}$$

where m_{KCl} is the mass of KCl in the solution, and $m_{\mathrm{H_2O}}$ is the mass of H_2O in the solution, at a temperature above freezing. Now we can calculate the amount of water that stays liquid in a closed system at a certain temperature T below freezing but above the eutectic temperature. For the actual temperature T we calculate the equilibrium salinity S_T at this temperature using (1), and from the mass of salt m_{KCl} in the solution we derive the amount of water $m_{l-\mathrm{H_2O}}$ that remains liquid for that temperature:

$$m_{l-\mathrm{H_2O}} = m_{\mathrm{KCl}} \frac{100\%}{S_T} - m_{\mathrm{KCl}}. \tag{3}$$

With (3) and the amount of water $m_{\mathrm{H_2O}}$ used to produce the initial solution, we calculate the mass of solid ice $m_{s-\mathrm{H_2O}}$:

$$m_{s-\mathrm{H_2O}} = m_{\mathrm{H_2O}} - m_{l-\mathrm{H_2O}}. \tag{4}$$

Where pure water freezes completely for temperatures ≤0 °C, a KCl solution starts to freeze partially at a salinity-dependent temperature below 0 °C and freezes completely at the eutectic temperature. Figure 1 shows the increase of ice content with decreasing temperature for various solutions. It is obvious that for a low initial salinity of 1 wt-% the slope of the curve is very steep close to the freezing point and small temperature changes have a strong effect on the ice content. Assuming that we are able to keep the temperature constant with an accuracy of ±0.05 °C in an experiment, we could still have a considerable error of about ±7% in the ice content for a solution with initially 1 wt-% KCl (see the dashed lines in Figure 1). Above 80% ice content the curve becomes much flatter and small temperature variations do not have a strong effect. For an initial salinity of 10 wt-% KCl the slope of the curve is generally flatter, but the maximum ice content is less than 50 wt-% at the eutectic point (see Figure 1). Depending on what ice content range is of interest, one has to choose the optimum initial salt concentration.

The volume of the salt solution changes when ice is formed (density of ice ρ_{ice} < density of water ρ_{W}). Considering a single pore in which an ice crystal starts to grow, solution has to be squeezed out of the pore in order to maintain the pore pressure at a constant level. Because the ice crystal consumes water from its immediate vicinity, the salt concentration will increase close to the crystal surface and a concentration gradient towards the outskirts of the pore will develop. For a slow temperature decrease, the crystal will grow slowly and the concentration gradient will be almost compensated by diffusion. For a fast-growing ice crystal the gradient will be stronger. The salt concentration of the water that is squeezed out of the pore volume, therefore, will depend on the formation characteristics (see Figure 2). To quantify the ice saturation of a drained porous system from the above formalism, we consider two extreme cases for a differential ice saturation increase $\Delta SAT_{\mathrm{ice}}$. Both cases rely on theoretical thought experiments to provide theoretical saturation limits.

1. Water with the average salt concentration of the pore water is squeezed out after ice formation (slow growth with compensated gradient). This is equivalent to ice formation in an *initially closed pore*. The

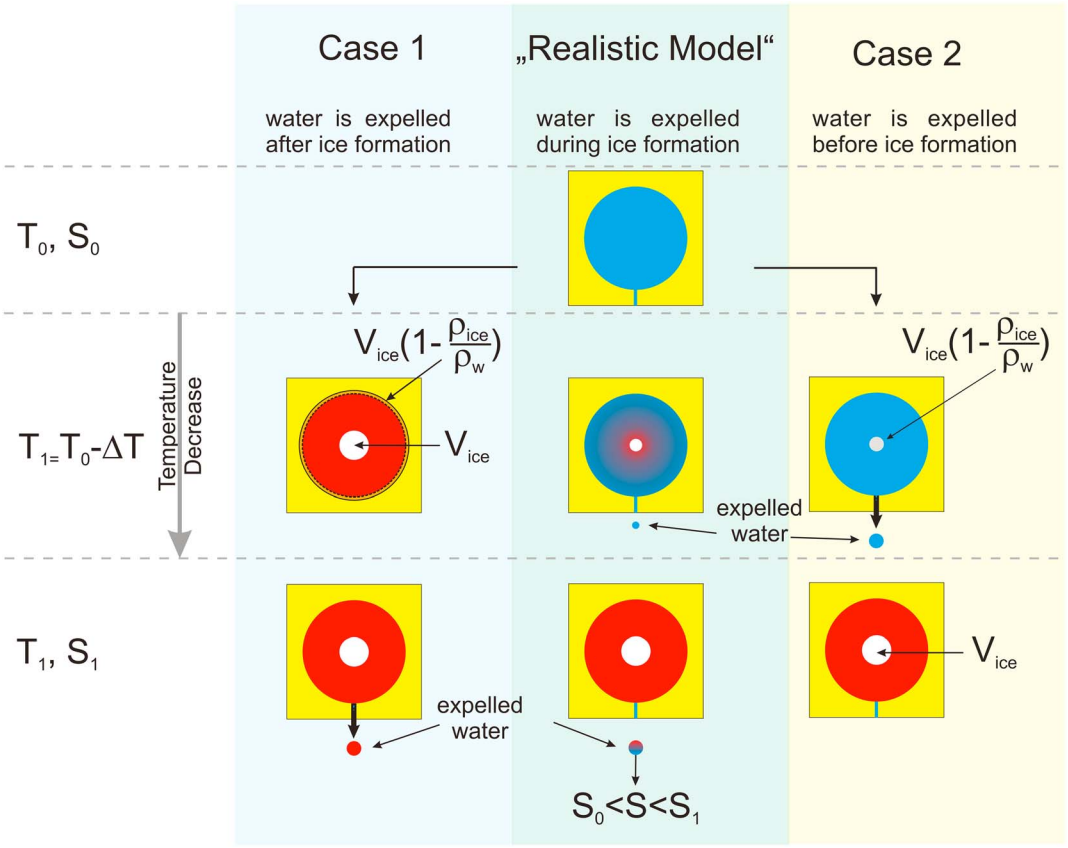

Figure 2. The limiting models where the water is expelled at the end of ice formation with the salinity S_1 (left), where the water is expelled before ice formation with the salinity S_0 (right), and a more realistic model where the water is expelled during the whole process of ice formation with a changing salinity (middle).

pore *expands* to maintain constant pressure and compensate for the volume increase ($V_{ice}(1 - \rho_{ice}/\rho_W)$) due to ice formation. After the concentration gradient has balanced, the *closed pore* opens, gets back to the original pore volume, and expels brine to keep the pressure constant.

2. The water is squeezed out with the salinity before the ice growth (fast growth in the pore center with strong salinity gradient towards the pore throats). This is equivalent to a situation where the water volume is expelled first, compensating for the entire volume expansion ($V_{ice}(1 - \rho_{ice}/\rho_W)$) during ice formation.

Figure 2 shows the extreme models for both approaches compared to a more likely model scenario. Since the salinity of the expelled water is different for the different models, and S_1 is determined by the temperature T_1 and therefore is the same for all models; the ice content and amount of expelled water must be different (see Figure 3).

Let us consider a pore volume V_{pore}, where SAT_w and SAT_{ice} are the water and ice saturations. The volume of the pore saturated with pore water is $V_{pore}SAT_w$. The sample is at a temperature T_0 equal to the freezing point depression for the salinity S_0 of the pore water. At this point the water saturation is $SAT_{w\text{-}0}$ and the ice saturation is $SAT_{ice\text{-}0} = 0$ with $1 = SAT_{w\text{-}0} + SAT_{ice\text{-}0}$. With the water density $\rho_{w\text{-}0}$ for that salinity and temperature, the total liquid mass in the pore is

$$m_{H_2O} + m_{KCl} = V_{pore}SAT_{w-0}\rho_{w-0} \;\; ; \;\; m_{H_2O} = m_{KCl}\frac{100\%}{S_0} - m_{KCl} \tag{5}$$

The salt amount in the pore is

$$m_{KCl} = \frac{V_{pore}SAT_{w-0}\rho_{w-0}S_0}{100\%}. \tag{6}$$

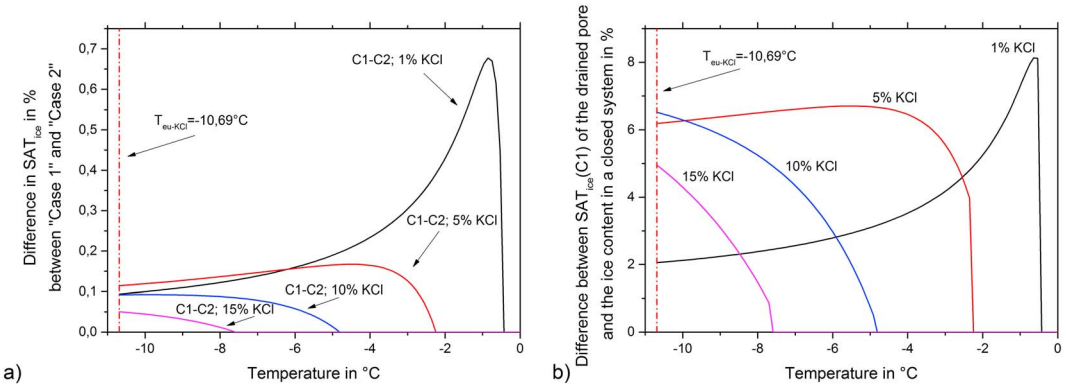

Figure 3. (a) Difference in ice saturation versus temperature between *case 1* and *case 2* (see description in the text) for different initial salinities. (b) Difference between the pore volume-related ice saturation (open drained system) and the mass-related ice content (closed system) for different initial salinities.

We assume a small temperature step of $-\Delta T$ that would result in a temperature $T_1 = T_0 - \Delta T$ causing ice formation which finally leads to a salinity increase to S_1, a density increase to $\rho_{w\text{-}1}$, and a decrease in water saturation $SAT_{w\text{-}1}$ ($\Delta T = 10.69 \cdot 10^{-3}$ °C was used for the calculations).

1. Case 1: We assume that the total amount of water contributes to the process of ice formation. The mass of total pore liquid and the mass of pure water that stays in the liquid phase is

$$m_{l-H_2O} + m_{KCl} = V_{pore} SAT^*_{w-1} \rho_{w-1}; m_{l-H_2O} = m_{KCl} \frac{100\%}{S_1} - m_{KCl}; \quad (7)$$

Since ice formation involves a volume expansion, we denote the water volume after ice formation with V_{pore} SAT^*_{w-1}. At this point the pore volume exceeds the sum of the pore constituents. The amount of water that is transformed into solid ice during the temperature step of ΔT ($m_{s\text{-}H2O}$, see equation (4)) equals the difference of (5) and (7), which can be calculated using (6) in the form

$$m_{s-H_2O} = V_{pore} SAT_{w-0} \rho_{w-0} S_0 \left(\frac{1}{S_0} - \frac{1}{S_1}\right) = V_{pore} \Delta SAT_{ice} \rho_{ice}; \Delta SAT_{ice} \rho_{ice} = SAT_{w-0} \rho_{w-0} - SAT^*_{w-1} \rho_{w-1}. \quad (8)$$

The increase in ice saturation of the pore is

$$\Delta SAT_{ice} = \frac{SAT_{w-0} \rho_{w-0}}{\rho_{ice}} \left(1 - \frac{S_0}{S_1}\right). \quad (9)$$

The resulting water and ice saturation in the pore after the excess water is expelled is

$$SAT_{w-1} = SAT_{w-0} - \Delta SAT_{ice} \;\; ; \;\; SAT_{ice-1} = SAT_{ice-0} + \Delta SAT_{ice}, \quad (10)$$

with a water mass of

$$V_{pore} SAT_{w-1} \rho_{w-1} = V_{pore} (SAT_{w-0} - \Delta SAT_{ice}) \rho_{w-1}. \quad (11)$$

Using equation (8) to eliminate ΔSAT_{ice}, we find

$$V_{pore} SAT_{w-1} \rho_{w-1} = V_{pore} \left(SAT^*_{w-1} - SAT_{w-0} \left(\frac{\rho_{w-0}}{\rho_{ice}} - 1\right)\right) \rho_{w-1} \quad (12)$$

and we can derive the expelled water volume to

$$V_{pore} (SAT^*_{w-1} - SAT_{w-1}) = SAT_{w-0} \left(\frac{\rho_{w-0}}{\rho_{ice}} - 1\right) V_{pore}. \quad (13)$$

When the excess water is squeezed out, the salt amount in the pore reduces to

$$m_{KCl} = \frac{V_{pore} SAT_{w-1} \rho_{w-1} S_1}{100\%}. \quad (14)$$

Since in reality the water expels simultaneously with the ice formation, less than the complete amount of pore water will be involved in the ice formation and the model for case 1 will slightly overestimate the ice saturation initially.

2. Case 2: The second thought experiment assumes that exactly that water volume is squeezed out with the original salinity that later, after the temperature drop, will be required by the volume expansion of the forming ice V_{ice} $(1 - \rho_{ice}/\rho_w)$.

The remaining mass of pore fluid in the pore is

$$m_{H_2O} + m_{KCl} = m_{KCl} \frac{100\%}{S_0} = V_{pore}(SAT_{w-0}\rho_{w-0} - \Delta SAT_{ice}\rho_{w-0} + \Delta SAT_{ice}\rho_{ice}) \quad (15)$$

and the amount of salt in the pore can be expressed by

$$m_{KCl} = \frac{S_0 V_{pore}(\rho_{w-0}(SAT_{w-0} - \Delta SAT_{ice}) + \Delta SAT_{ice}\rho_{ice})}{100\%}. \quad (16)$$

The mass of pore fluid that remains in the liquid phase after ice formation is

$$m_{H_2O-I} + m_{KCl} = m_{KCl} \frac{100\%}{S_1} = V_{pore}(SAT_{w-0}\rho_{w-0} - \Delta SAT_{ice}\rho_{ice}) \quad (17)$$

The amount of water transformed into a solid ice phase is the difference of equations (15) and (17):

$$m_{s-H_2O} = V_{pore}\Delta SAT_{ice}\rho_{ice} = V_{pore} S_0(\rho_{w-0}(SAT_{w-0} - \Delta SAT_{ice}) + \Delta SAT_{ice}\rho_{ice})\left(\frac{1}{S_0} - \frac{1}{S_1}\right), \quad (18)$$

Reorganizing (18) to isolate the increase in ice saturation of the pore results in

$$\Delta SAT_{ice} = \frac{SAT_{w-0}\rho_{w-0}}{\rho_{ice}\left(\frac{1}{1-\frac{S_0}{S_1}} + \frac{\rho_{w-0}}{\rho_{ice}} - 1\right)} \quad (19)$$

For high ice formation rates and low ice to water ratios in the pore the second approach should be more realistic, especially for high growth rates under laboratory conditions. For high ice saturations and low water to ice ratios in the pore, the expelled water will probably be influenced by the salinity increase due to ice formation. However, approach 2 probably better reflects the laboratory conditions.

The difference between both approaches is generally below 1% and decreases with increasing salinity, with decreasing temperature, and with decreasing temperature increments (Figure 3a). For practical applications it is of no consequence which approach is chosen. However, it is important to convert the mass related ice content (see Figure 1) into a pore volume related ice saturation using one of the above described approaches. The difference between mass-related ice content and pore volume-related ice saturation can easily exceed 5% (see Figure 3b). For the conversion we used the dependence of water density on salinity at associated freezing point in the form (see section 3)

$$\rho_w = 8.587\ 10^{-6} S^2 + 6.62\ 10^{-3} S + 0.99984 \quad (20)$$

3. Experimental Procedure and Results

3.1. Density and Conductivity of a KCl Solution at Freezing Point

Using the approach presented above, we require the solution density dependence on the freezing point depression temperature to calculate the ice saturation of the sample. To the best of our knowledge, these

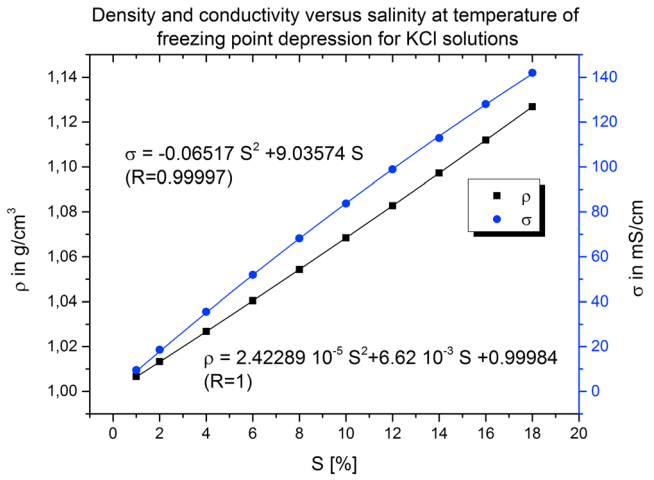

Figure 4. Density and electrical conductivity as a function of salinity of a KCl solution measured at the corresponding freezing point of the solution (see Table 1).

data have not been published. Thus, we measured the density of the KCl solution as a function of freezing point using buoyancy measurements with a defined glass volume submerged in the solution. Simultaneously, we determined the electrical conductivity at the freezing point temperature for KCl solutions (Figure 4) as a prerequisite for the interpretation of electrical resistivity measurements. We produced the KCl solution from distilled, degassed water and calculated the freezing point depression for the given salinity using (1). The weighted glass beaker containing about 1 l of the KCl solution was placed in a thermostated bath. We installed a scale (Mettler PM2000) with an underfloor mounting option above the bath thermostat (LAUDA ECO RE 1050). The glass volume was attached to the scale and submerged in the KCl solution in the thermostated bath through a hole in the lid of the bath. We measured the buoyancy when temperature had equilibrated and the scale reading remained constant over a time of at least 1 hr at the freezing point depression temperature. Knowing the mass and the volume of the glass body, we were able to calculate the solution density from the measured buoyancy. The precision of the scale is 0.01 g, and the immersion volume is 116.64 cm^3, which results in density resolution of about 0.0001 g/cm^3. The conductivity was measured with a conductivity meter (WTW Cond 3310 with Tetracon 325 electrode). The measured values are given in Table 1 and are depicted in Figure 4. For the ice saturation calculations we used the correlation equations given in Figure 4.

3.2. Experimental Setup

For the experiments on the dependence of compressional-wave velocity on ice saturation we used the standard thermostated oil pressure system (system for experimental petrophysics—SEPP). SEPP consists of an autoclave with a heating/cooling jacked containing the sample setup. The inner diameter is 70 mm, and the usable length of the vessel is 250 mm. It is designed for a maximum pressure of 80 MPa. The sample setup is mounted at the top closure of the autoclave containing the feedthroughs for confining pressure oil, pore fluid inlet and pore fluid outlet, and the signal lines (see Figure 5). The sample is separated from the confining pressure oil by means of a Viton jacket and the Hastelloy end caps. The end caps contain the *P* and *S* wave transducers for velocity measurements and are used as current electrodes. The Viton jacket contains up to four potential electrodes for the resistivity measurements and to assess the homogeneity of the sample. A resistive length sensor is mounted between the end caps to record changes in sample length. To control the sample temperature, a Pt100 temperature sensor is attached to the Viton jacket. The fluid feedthroughs in the end caps allow for pumping the pore fluid through the sample, to apply a certain pore pressure or to exchange the pore fluid. To simulate in situ pressure and temperature conditions, the autoclave is connected to a confining pressure syringe pump (ISCO 100DM) and to a thermostat (Huber K6 s-CC-NR; see Figure 5).

3.3. Experimental Procedure

We started the experiment with a dry sand sample (beach sand, Warnemünde/Baltic Sea) which was set to the desired confining pressure (10 MPa; ISCO 100DM) to measure the compressional-wave velocities in the dry state. The velocity data of the dry sample is required for fluid substitution calculations using Gassmanns's theory (e.g., Mavko et al., 2009; Schön, 1996). We used a HPLC (Knauer Smartline 100) pump to saturate the initially evacuated sand sample with a degassed KCl solution. To ensure complete saturation, 10 to 20 pore volumes were exchanged at room temperature. Next, we switched the pump off and measured

Table 1
Freezing Point, Density, and Electrical Conductivity for Different Salinities of a KCl Solution

S in %	1	2	4	6	8	10	12	14	16	18
T_{FP} (°C)	−0.46	−0.92	−1.85	−2.80	−3.78	−4.80	−5.86	−6.98	−8.17	−9.44
ρ (g/cm^3)	1.0066	1.0133	1.0268	1.0405	1.0543	1.0684	1.0827	1.0972	1.1120	1.1269
σ (mS/cm)	9.47	18.58	35.5	51.9	68.2	83.7	98.9	112.9	128	142

Note. The freezing point depression is calculated using equation (1); the densities and conductivities are measured (see text for detailed description and Figure 4).

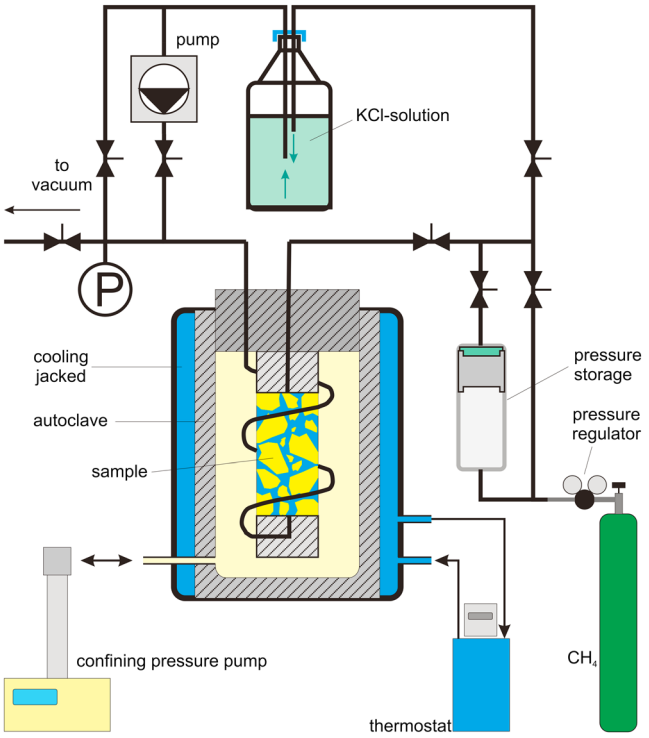

Figure 5. General concept of the experimental setup of SEPP-hydrate (system for experimental petrophysics) used for the experiments (see text for a more detailed description).

the mass loss of the fluid in the reservoir to determine the pore volume of the installed sand sample. From the sand mass, the grain density, and the pore volume we estimated the porosity at 37%. After the measurement of the compressional-wave velocity for the fully brine-saturated state we set the sample to different temperatures between 0 °C and −15 °C (complete freezing) in order to observe the velocity as a function of ice content. To keep the temperature gradient inside the sample low during freezing and to have comparable conditions between different experiments, we worked with a temperature ramp of 0.1 °C/hr. The pore pressure inlet and outlet was kept open during freezing to allow drainage into the brine reservoir. The temperature at the sample surface was monitored using the Pt100 RTD. In order to assess when the temperature equilibrium inside the sample is reached and ice formation is complete, the resistivity of the sample is logged with a four-electrode arrangement (see Figure 6). The heat generated by ice formation dissipates over the sample surface, and a constant temperature indicates the end of ice formation. This is confirmed by the maximum in electrical sample resistance. The slight decrease in resistance is probably caused by recrystallization due to Oswald ripening and an equilibration of ion concentration gradients in the pore fluid. When the resistance has almost equilibrated, we perform the compressional-wave velocity measurement. The equilibrated sample temperature is determined as a prerequisite for the determination of the ice saturation. It should be mentioned that the velocity remains constant shortly after the temperature has equilibrated and is obviously not as sensitive to ice recrystallization or salinity equilibration. The thermostat is set to the next temperature, and the new measurement is taken when the temperature has equilibrated or the resistivity remains almost constant. In this experiment we measured with a 5% KCl solution as a compromise to get reasonably accurate ice saturation while maximizing the ice saturation. If one aims for the dependence until very high saturation of about 90% and more, it is advisable to perform a two-stage experiment with fluid exchange; use high salinity to get high accuracy at low ice contents and a low concentration solution to get a very high final ice saturation (see Figure 1 and section 2). The time needed for the fluid substitution process depends on the mean grain size and the grain size distribution. For permeable clean sand it is possible within a day. The resistivity log would indicate when the old fluid has been replaced and a new constant resistivity is established in the sample.

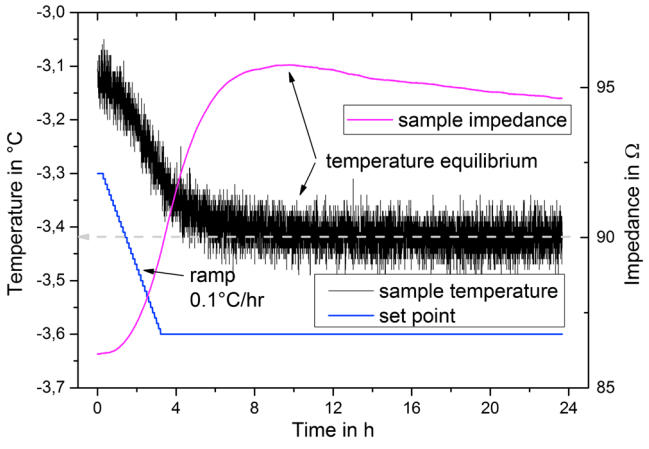

Figure 6. Temperature measured at the sample surface and sample impedance as a function of time after the temperature was set to a lower value with a ramp of 0.1 °C/hr to increase the ice content of the sample.

Figure 7 shows the measured compressional-wave velocities as a function of ice saturation in the sand and as function of methane hydrate content in a glass bead sample (Spangenberg et al., 2008). In the glass bead sample the hydrate was formed from methane dissolved in water. Based on the measurements on the dry and water-saturated sample, we did a fluid substitution calculation assuming a water hydrate suspension as pore fill. The measurements follow the trend of the modeled curve very well up to a saturation of about 40%. For higher saturations the measured data show a stronger velocity increase compared to the modeled velocities. This change is the result of the originally *pure* pore-filling crystals starting to become a load-bearing framework. This transition from pore-filling to pore-filling and load-bearing habit has also been observed for sand tetrahydrofuran-hydrate systems (Yun et al., 2005). The results show that ice forms generally as a noncementing phase in the pores and provides an easy analogue for the influence of pore-filling and load-bearing methane hydrate on the compressional-wave velocities of sandy sediments.

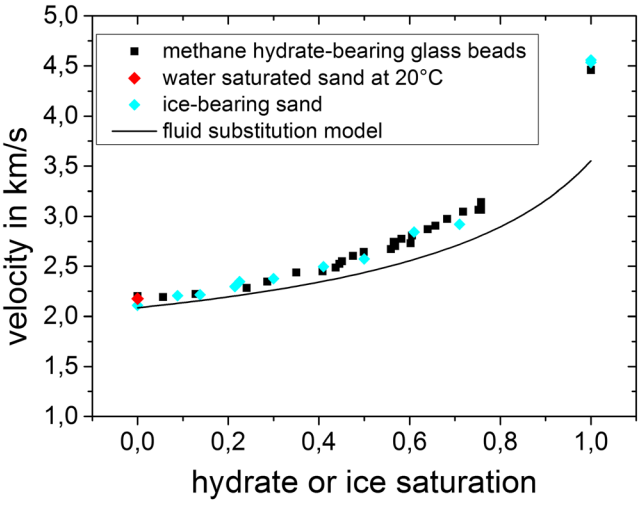

Figure 7. Velocities of the ice-bearing beach sand and a hydrate-bearing glass bead sediment as a function of ice and hydrate saturation, respectively. Ice and hydrate obviously have a similar influence on the velocity of porous sediments.

During the experiments we recognized that the absorption of wave energy increases with ice content. This is a special feature which has also been observed in natural hydrate-bearing formations, where a velocity increase due to higher hydrate concentrations is associated with strong absorption in the seismic frequency range and is also seen for the higher frequencies of sonic log measurements (e.g., Bauer et al., 2005; Guerin et al., 2005). This is another qualitative indicator that supports our assumption that ice can be used as an easy to handle analogue for the study of seismic properties in hydrate-bearing formations.

The good analogy we found for the compressional-wave velocity of hydrate- and ice-bearing sediments, we could not yet determine for the electrical measurements. The measured electrical resistivity of the ice-bearing sediment and the dependence we found for the glass bead sediment, where the hydrate was formed from methane dissolved in water (Spangenberg & Kulenkampff, 2006), are different. For the ice-bearing sediment we found a strong correlation between resistivity and water saturation, which could be used to derive Archie's saturation coefficient (e.g., Schön, 1996, and references therein) to a value of $n = 1.85$ which is close to Pearson's average of 1.938 over different lithologies. For methane hydrate in a glass bead sediment we observed a dependence of the saturation exponent on hydrate saturation as predicted by a simple sphere pack model for hydrate-bearing sediments (Spangenberg, 2001; Spangenberg & Kulenkampff, 2006). One reason for the observed difference could be related to the stronger structured surface topology of the natural quartz sand compared to the sphere pack resulting in a more complex geometry of the conducting pore-water network (Figure 8). But it might also be related to the strongly different formation kinetics. In contrast to ice formation, hydrate formation from dissolved methane is very slow and limited by the low methane availability (low methane solubility).

4. Discussion

We applied Pearson's idea (Pearson et al., 1983) to use ice as an analogue for methane hydrate to simplify the experimental procedure for lab studies on the seismic properties of hydrate-bearing sandy sediments. Our approach differs from Pearson's approach in (1) the way the ice concentration is determined and (2) that we compare the velocities measured on ice-bearing sand with data produced on hydrate-bearing sediments in which methane hydrate was produced from methane dissolved in water. This comparison clearly shows that ice and hydrate forming without a free gas phase present in the porous system results in a pore-filling or pore-filling and load-bearing habitus. For compressional-wave velocities, ice formation from a salt solution can be used as an analogue for methane hydrate. This provides an option to produce data on the dependence of compressional-wave velocity on *hydrate* saturation much faster with less complex experimental systems.

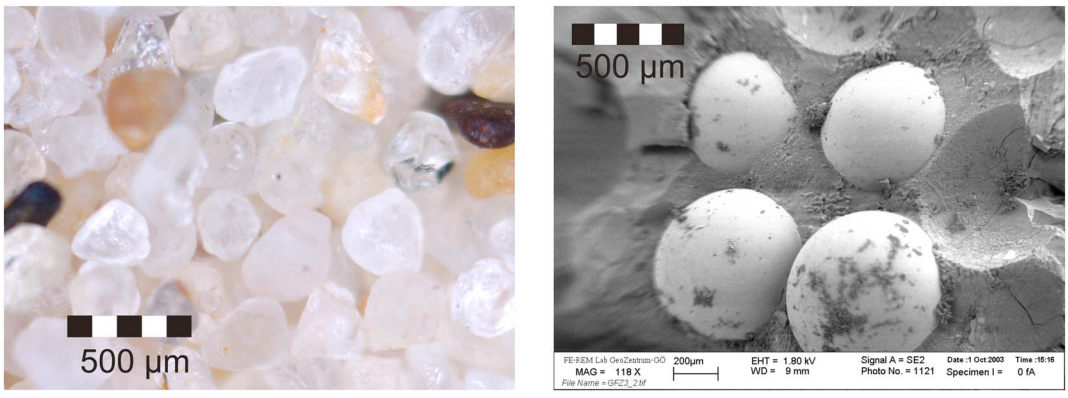

Figure 8. Beach sand used for the ice experiments (left) and a scanning electron microscope image of glass beads embedded in a matrix of 83% methane hydrate and 17% ice (Spangenberg et al., 2005).

The qualitative observation we have from hydrate-bearing formations and our ice experiments support the applicability of the method to study the absorption of *P* wave energy and its dependence on ice or hydrate concentration in a systematic way.

The interpretation of electrical resistivity measurements with respect to hydrate concentration is to date mainly conducted using Archie's equation with the saturation exponent of $n = 1.9386$, as proposed by Pearson et al. (1983) (e.g., Collett & Dallimore, 1998; Spangenberg, 2001). Using ice as analogue for hydrate, we found a dependence of resistivity on ice saturation that could be correlated with Archie's equation using $n = 1.85$. This value is lower than the average of 1.9386 but is higher than the value of $n = 1.715$ given by Pearson et al. (1983) for unconsolidated material. Besides this, saturation exponents derived from field experiments indicate that the value of $n = 1.9386$ is too low. Malinverno et al. (2008) determined $n = 2.42$ from pore water chlorinity measurements and resistivity logs in a hydrate-bearing sand at Cascadia Margin. Cook and Waite (2018) determined hydrate saturation from sonic log and derived *n* values from the resistivity log for the hydrate-bearing formations in the Mallik 5 L-38 research well and in hydrate-bearing sands of two wells drilled within the Gulf of Mexico Gas Hydrate Joint Industry Project (see, for instance, Boswell et al., 2012; Collett et al., 2012). Based on their extensive calibration work Cook and Waite (2018) recommend the value of $n = 2.5 \pm 0.5$ in hydrate-bearing sands in marine or permafrost settings, if no site specific calibration for *n* is available. Additionally, their paper provides a comprehensive overview about the variability of *n* determined in the field and with different methods in laboratory studies.

The question of whether ice can be used as an analogue for methane hydrate to investigate its influence on the electrical resistivity is obviously just one part of the more complex problem to understand the influence of the hydrate or ice framework within the brine-filled pore network on the resulting electrical properties. What influences the structure of this framework and how it is related to the formation kinetics of hydrate or ice? Besides growth kinetics, concentration and temperature gradients in lab experiments often do not really simulate the natural situation. What influence these different *lab conditions* have and if they can explain the above described discrepancies are just some of the questions that deserve more attention in future studies.

5. Conclusions

We were interested in measuring dependencies of compressional-wave velocity and electrical resistivity on hydrate saturation within sand sediments. Because the formation of methane hydrate in the pore space of a sand sample is both complicated and time consuming, we developed a quick look method using ice as a proxy for methane hydrate. The presented method and the measured data show the following:

The dependence of freezing point depression of a salt solution on salt concentration can be used to calculate the ice saturation. However, it requires a correction of the amount of water expelled from the sediment due to the volume expansion of the forming ice. For the correction the density dependence of the saline solution on salt concentration at freezing point needs to be known. We provide the data for a KCl solution.

Ice grown from a salt solution in the pore space of a sandy sediment forms as a noncementing pore-filling solid phase and at higher saturations as a pore-filling and load-bearing solid phase like methane hydrate.

The compressional-wave velocities measured on an ice-bearing sample compare very well with those measured with methane hydrate as pore-fill.

The measurement of a full dependency on saturation up to 90% with ice can be done in less than 25% of the time required for the same dependency with gas hydrate formed from methane dissolved in water.

Ice can be formed in the pore space of a sand sample without a complicated pore pressure system, which would be necessary for the formation of a methane hydrate-bearing sample under laboratory conditions.

Acknowledgments
We are very grateful to Ronny Giese for the support during the preparation and execution of the experiments. The authors thank the staff of the GFZ workshops for their invaluable technical support. The authors thank Ann Cook and William Waite for their very constructive and helpful reviews of this work. We also gratefully acknowledge the financial support from the German Federal Ministry for Economic Affairs and Energy and the German Federal Ministry of Education and Research within the project SUGAR (research grants 03SX320E and 03G0856C). The data used are listed in the text, the table, and the references.

References

Archie, G. E. (1942). The electrical resistivity log as an aid in determining some reservoir characteristics. *Transactions of AIME*, *146*(01), 54–62. https://doi.org/10.2118/942054-G

Bauer, K., Haberland, C., Pratt, R. G., Hou, F., Medioli, B. E., & Weber, M. H. (2005). Ray-based cross-well tomography for *P*-wave velocity, anisotropy, and attenuation structure around the JAPEX/JNOC/GSC et al. Mallik 5L-38 gas hydrate production research well. *Bulletin - Geological Survey of Canada*, *585*, 121.

Boswell, R. (2009). Is gas hydrate energy within reach? *Science*, *325*(5943), 957–958. https://doi.org/10.1126/science.1175074

Boswell, R., Collett, T. S., Frye, M., Shedd, W., McConnell, D. R., & Shelander, D. (2012). Subsurface gas hydrates in the northern Gulf of Mexico. *Marine and Petroleum Geology*, *34*(1), 4–30. https://doi.org/10.1016/j.marpetgeo.2011.10.003

Boswell, R., Yamamoto, K., Lee, S. R., Collett, T., Kumar, P., & Dallimore, S. (2014). *Methane hydrates. Future energy: Improved, sustainable and clean options for our planet, 2nd ed.* (pp. 159–178). London: Elsevier. https://doi.org/10.1016/B978-0-08-099424-6.00008-9

Choi, J. H., Dai, S., Cha, J. H., & Seol, Y. (2014). Laboratory formation of noncementing hydrates in sandy sediments. *Geochemistry, Geophysics, Geosystems*, *15*, 1648–1656. https://doi.org/10.1002/2014GC005287

Collett, T. S., & Dallimore, S. R. (1998). *Quantitative assessment of gas hydrates in the Mallik L-38 Well, Mackenzie Delta, NWT, Canada*. In Proceedings of the 7th International Conference on Permafrost, Yellowknife, Canada.

Collett, T. S., Lee, M. W., Zyrianova, M. V., Mrozewski, S. A., Guerin, G., Cook, A. E., & Goldberg, D. S. (2012). Gulf of Mexico Gas Hydrate Joint Industry Project Leg II logging-while-drilling data acquisition and analysis. *Marine and Petroleum Geology*, *34*(1), 41–61. https://doi.org/10.1016/j.marpetgeo.2011.08.003

Cook, A. E., & Waite, W. F. (2018). Archie's saturation exponent for natural gas hydrate in coarse-grained reservoirs. *Journal of Geophysical Research: Solid Earth*, *123*, 2069–2089. https://doi.org/10.1002/2017JB015138

Cortes, D. D., Martin, A. I., Yun, T. S., Francisca, F. M., Santamarina, J. C., & Ruppel, C. (2009). Thermal conductivity of hydrate-bearing sediments. *Journal of Geophysical Research*, *114*, B11103. https://doi.org/10.1029/2008JB006235

Guerin, G., Goldberg, D., & Collett, T. S. (2005). Sonic attenuation in the JAPEX/JNOC/GSC et al. Mallik 5L-38 gas hydrate production research well. *Bulletin-Geological Survey of Canada*, *585*, 117.

Hall, D. L., Sterner, S. M., & Bodnar, R. J. (1988). Freezing point depression of NaCl-KCl-H_2O solutions. *Economic Geology*, *83*(1), 197–202. https://doi.org/10.2113/gsecongeo.83.1.197

Handa, Y. P., Hawkins, R. E., & Murray, J. J. (1984). Calibration and testing of a Tian-Calvet heat flow calorimeter. Enthalpies of fusion and heat capacities for ice and THF hydrate in the range 85 to 270 K. *The Journal of Chemical Thermodynamics*, *16*, 623–632. https://doi.org/10.1016/0021-9614(84)90042-9

Hyodo, M., Li, Y., Yoneda, J., Nakata, Y., Yoshimoto, N., Nishimura, A., & Song, Y. (2013). Mechanical behavior of gas-saturated methane hydrate-bearing sediments. *Journal of Geophysical Research: Solid Earth*, *118*, 5185–5194. https://doi.org/10.1002/2013JB010233

Inada, N., & Yamamoto, K. (2015). Data report: Hybrid Pressure Coring System tool review and summary of recovery result from gas-hydrate related coring in the Nankai project. *Marine and Petroleum Geology*, *66*, 323–345. https://doi.org/10.1016/j.marpetgeo.2015.02.023

Kvenvolden, K. A. (1988). Methane hydrate—A major reservoir of carbon in the shallow geosphere? *Chemical Geology*, *71*(1–3), 41–51. https://doi.org/10.1016/0009-2541(88)90104-0

Lee, J. Y., Yun, T. S., Santamarina, J. C., & Ruppel, C. (2007). Observations related to tetrahydrofuran and methane hydrates for laboratory studies of hydrate-bearing sediments. *Geochemistry, Geophysics, Geosystems*, *8*, Q06003. https://doi.org/10.1029/2006GC001531

Malinverno, A., Kastner, M., Torres, M. E., & Wortmann, U. G. (2008). Gas hydrate occurrence from pore water chlorinity and downhole logs in a transect across the northern Cascadia margin (Integrated Ocean Drilling Program Expedition 311). *Journal of Geophysical Research*, *113*, B08103. https://doi.org/10.1029/2008JB005702

Mavko, G., Mukerji, T., & Dvorkin, J. (2009). *The rock physics handbook: Tools for seismic analysis of porous media*. New York: Cambridge University Press. https://doi.org/10.1017/CBO9780511626753

Pearson, C. F., Halleck, P. M., McGuire, P. L., Hermes, R., & Mathews, M. (1983). Natural gas hydrate deposits: A review of in situ properties. *The Journal of Physical Chemistry*, *87*(21), 4180–4185. https://doi.org/10.1021/j100244a041

Priest, J. A., Rees, E. V., & Clayton, C. R. (2009). Influence of gas hydrate morphology on the seismic velocities of sands. *Journal of Geophysical Research*, *114*, B11205. https://doi.org/10.1029/2009JB006284

Santamarina, J. C., & Ruppel, C. (2010). The impact of hydrate saturation on the mechanical, electrical, and thermal properties of hydrate-bearing sand, silts, and clay. In M. Riedel, E. C. Willoughby, & S. Chopra (Eds.), *Geophysical characterization of gas hydrates*, *Geophysical Development Series* (Vol. 14, pp. 373–384). Tulsa, OK: Society of Exploration Geophysicists. https://doi.org/10.1190/1.9781560802197.ch26

Schön, J. H. (1996). Handbook of geophysical exploration: Seismic exploration. In *Physical properties of rocks: Fundamentals and principles of petrophysics* (Vol. 18, pp. 249–252). Amsterdam: Elsevier

Schultheiss, P., Holland, M., & Humphrey, G. (2009). Wireline coring and analysis under pressure: Recent use and future developments of the HYACINTH system. *Scientific Drilling*, *7*, 44–50. https://doi.org/10.2204/iodp.sd.7.07.2009

Schultheiss, P., Holland, M., Roberts, J., Huggett, Q., Druce, M., & Fox, P. (2011). *PCATS: Pressure core analysis and transfer system*. In Proceedings of the 7th International Conference on Gas Hydrates (ICGH 2011) (pp. 17–21). Edinburgh, UK.

Spangenberg, E. (2001). Modeling of the influence of gas hydrate content on the electrical properties of porous sediments. *Journal of Geophysical Research*, *106*(B4), 6535–6548. https://doi.org/10.1029/2000JB900434

Spangenberg, E., Beeskow-Strauch, B., Luzi, M., Naumann, R., Schicks, J. M., & Rydzy, M. (2008). *The process of hydrate formation in clastic sediments and its impact on their physical properties*. In Proceedings of the 6th International Conference on Gas Hydrates.

Spangenberg, E., & Kulenkampff, J. (2006). Influence of methane hydrate content on electrical sediment properties. *Geophysical Research Letters*, *33*, L24315. https://doi.org/10.1029/2006GL028188

Spangenberg, E., Kulenkampff, J., Naumann, R., & Erzinger, J. (2005). Pore space hydrate formation in a glass bead sample from methane dissolved in water. *Geophysical Research Letters*, *32*, L24301. https://doi.org/10.1029/2005GL024107

Spangenberg, E., Priegnitz, M., Heeschen, K., & Schicks, J. M. (2014). Are laboratory-formed hydrate-bearing systems analogous to those in nature? *Journal of Chemical & Engineering Data*, *60*(2), 258–268. https://doi.org/10.1021/JE5005609

Strauch, B., Schicks, J. M., Luzi-Helbing, M., Naumann, R., & Herbst, M. (2018). The difference between aspired and acquired hydrate volumes—A laboratory study of THF hydrate formation in dependence on initial THF: H_2O ratios. *The Journal of Chemical Thermodynamics*, *117*, 193–204. https://doi.org/10.1016/j.jct.2017.09.013

Waite, W. F., Santamarina, J. C., Cortes, D. D., Dugan, B., Espinoza, D. N., Germaine, J., et al. (2009). Physical properties of hydrate-bearing sediments. *Reviews of Geophysics*, *47*, RG4003. https://doi.org/10.1029/2008RG000279

Waite, W. F., & Spangenberg, E. (2013). Gas hydrate formation rates from dissolved-phase methane in porous laboratory specimens. *Geophysical Research Letters*, *40*, 4310–4315. https://doi.org/10.1002/grl.50809

Waite, W. F., Winters, W. J., & Mason, D. H. (2004). Methane hydrate formation in partially water-saturated Ottawa sand. *American Mineralogist*, *89*(8–9), 1202–1207. https://doi.org/10.2138/am-2004-8-906

Yun, T. S., Francisca, F. M., Santamarina, J. C., & Ruppel, C. (2005). Compressional and shear wave velocities in uncemented sediment containing gas hydrate. *Geophysical Research Letters*, *32*, L10609. https://doi.org/10.1029/2005GL022607